ACS Catalysis

Letter

Cite This: ACS Catal. 2019, 9, 98−104

pubs.acs.org/acscatalysis

Alkyne-Functionalized Ruthenium Nanoparticles: Impact of Metal−Ligand Interfacial Bonding Interactions on the Selective Hydrogenation of Styrene

Fengqi Zhang,[†,¶] Jingjing Fang,[†,¶] Lin Huang,[†,¶] Wenming Sun,[‡] Zhang Lin,[§] Zhenqing Shi,[§] Xiongwu Kang,*[,†] and Shaowei Chen*[,†,∥]

[†]Guangzhou Key Laboratory for Surface Chemistry of Energy Materials, New Energy Research Institute, School of Environment and Energy, South China University of Technology, Guangzhou Higher Education Mega Centre, Guangzhou 510006, China

[‡]State Key Laboratory of Green Building Materials, China Building Materials Academy, Beijing 100041, China

[§]Guangdong Engineering and Technology Research Center for Environmental Nanomaterials, School of Environment and Energy, South China University of Technology, Guangzhou, Guangdong 510006, China

[∥]Department of Chemistry and Biochemistry, University of California, 1156 High Street, Santa Cruz, California 95064, United States

Supporting Information

ABSTRACT: In the present study, ruthenium nanoparticles functionalized with terminal and internal alkynes were prepared, and it was found that internal alkynes formed a η^2 side-on configuration on the surface of ruthenium nanoparticles, in sharp contrast to the ruthenium-vinylidene interfacial bonds for terminal alkynes. For the nanoparticles capped with terminal alkyne, hydrogenation of both the vinyl moiety and phenyl ring occurred, whereas selective hydrogenation of the vinyl moiety was observed with internal alkyne-functionalized nanoparticles. This work highlights the importance of the metal−organic interface in the rational design and engineering of the nanoparticle catalyst for organic synthesis.

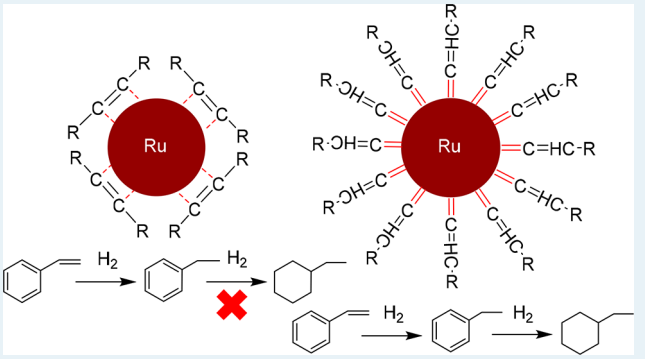

KEYWORDS: *ruthenium nanoparticles, internal alkyne, η^2 side-on configuration, $\sigma-\pi$ covalent, interfacial charge transfer, styrene hydrogenation*

INTRODUCTION

Catalysis plays a critical role in the production and transformation of valuable chemicals, where high selectivity toward the desired molecules and compounds significantly reduces the amount of chemical wastes generated and represents an important part in the quest for "green chemistries".[1−4] Toward this end, a range of synthetic approaches based on nanotechnology have been reported in recent literature.[5] Among them, surface functionalization of transition-metal nanoparticles by selecting organic capping ligands has been demonstrated to be a powerful tool in the manipulation and enhancement of the nanoparticle catalytic performance.[6−11] For instance, as one of the capping ligands, terminal alkyne molecules have been demonstrated to be effective in modulating the catalytic activity of the metal nanoparticles in heterogeneous catalysis. For instance, rod-shaped $[Au_{25}(PPh_3)_{10}(C{\equiv}CPh)_5X_2]^{2+}$ (X = Br, Cl) nanoclusters exhibited selective catalytic activity toward the semihydrogenation of terminal alkynes because of bridging of Au atoms by deprotonated alkynes, while the uncapped Au nanoclusters are active in the hydrogenation of both terminal and internal alkynes.[12] In another study,[13] the formation of surface staple motifs of PhC≡C−Au−C≡CPh in alkynyl-protected $Au_{34}Ag_{28}(PhC{\equiv}C)_{34}$ nanoclusters led to enhanced catalytic performance toward the hydrolytic oxidation of organosilanes to silanols, in comparison to those with the surface ligands partially or completely removed. Wang's group compared the catalytic activity of alkyne- and thiolate-capped Au_{38} nanoclusters in the semihydrogenation of alkynes to alkenes and observed markedly higher activity of the former (>97%) than that of the latter (<2%).[14] However, studies of the functionalization of a transition metal nanoparticle by internal alkynes have been scarce. There are at least two immediate differences of the interfacial bonding interactions, as compared to those with terminal alkynes. One is the metal−ligand interfacial bonding configuration and the other is the packing of organic ligands on the nanoparticle surface; both factors are likely to impact the interactions of metal nanoparticles with

Received: October 6, 2018
Revised: November 29, 2018
Published: November 30, 2018

DOI: 10.1021/acscatal.8b04028
ACS Catal. 2019, 9, 98−104

Scheme 1. Preparation and Interfacial Bonding Interactions of Terminal and Internal Alkyne Capped Ruthenium Nanoparticles

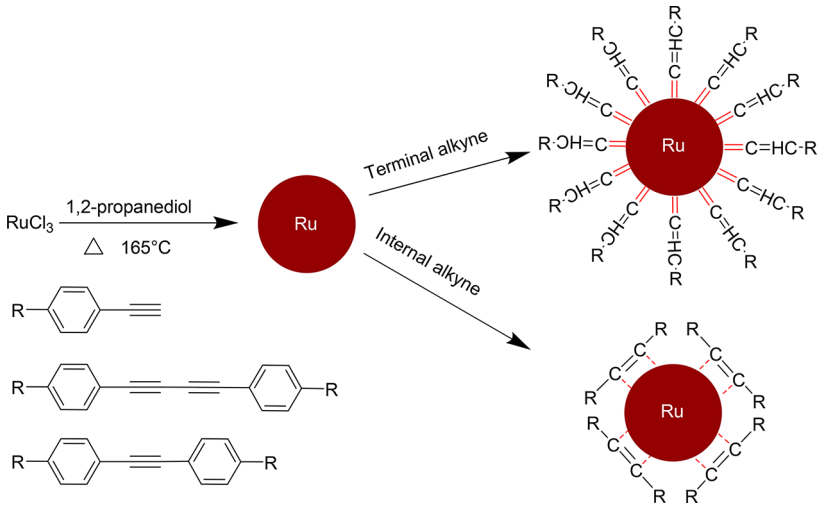

reaction species and hence the catalytic performance. In addition, ruthenium (Ru), as the most active catalyst for the Fischer−Tropsch reaction[15] and hydrogenation of olefin and aromatics,[16] has been widely studied. Most importantly, ruthenium demonstrates unique chemistry when interacting with nonmetal elements, such as the formation of Ru═carbene double bonds[17] and the tautomerization through 1,3-hydrogen shift/l,2- hydrogen shift and the formation of Ru═vinylidene bonds[18] when terminal alkynes assemble on the Ru metal surface. Ruthenium nanoparticles passivated with such unique metal−ligand interfacial bonds may therefore demonstrate unique physical and chemical properties.

Herein, ruthenium nanoparticles capped with terminal alkynes and internal alkynes were prepared (Scheme 1), and the impacts of the ruthenium-ligand interfacial bonds on the hydrogenation of styrene were also examined. It was found that internal alkynes most likely adopted the η^2 side-on mode through $\delta-\pi$ covalent bonds on the Ru nanoparticle surfaces, in contrast to the end-on ruthenium-vinylidene bonds formed with terminal alkynes. Interestingly, Ru nanoparticles capped with internal alkyne moieties exhibited markedly higher selectivity toward vinyl hydrogenation of styrene than that of terminal counterparts.

RESULTS AND DISCUSSION

Ruthenium nanoparticles were capped with 1-ethynyl-4-hexylbenzene (EHB, a terminal alkyne), 1,2-bis(4-hexylphenyl)ethyne (BEHB, an internal alkyne) 1,4-bis(4-hexylphenyl)buta-1,3-diyne (DEHB, internal diyne), 1-dodecyne (HC12, a terminal alkyne), and phenylethanethiol (PThiol) and denoted as Ru@EHB, Ru@BEHB, Ru@DEHB, Ru@HC12, and Ru@PThiol, respectively (Figure S1−3). The diameters of Ru nanoparticles were derived from the TEM images shown in Figure S4, which are very similar at 1.4 ± 0.3, 1.7 ± 0.3, and 1.7 ± 0.3 nm for Ru@EHB, Ru@BEHB, and Ru@DEHB, respectively.

The TGA and ICP-MS measurements of both the capping ligands and the Ru nanoparticles were shown in Figure S5, Table 1 and Table S1. The footprint of the corresponding ligand on the ruthenium core surface was estimated to be 10.7 Å^2 for Ru@EHB, 27.2 Å^2 for Ru@BEHB, and 64.4 Å^2 for Ru@DEHB. Since the steric hindrance of capping ligands in the side-on mode was much larger than that in the end-on mode, the footprint of the former capping ligands would be larger than that of the latter. Here the footprint of each hexylbenzene moiety on Ru@BEHB was larger than that of Ru@EHB, suggesting that the terminal alkynes take the end-on mode while internal alkynes adopt the side-on mode on Ru nanoparticle surface (Scheme 1). Since DEHB has two conjugated C≡C triple bonds and needs more space than single C≡C triple bond of BEHB when adsorbed on the surface of Ru nanoparticles in the side-on mode, the footprint of DEHB shall be more than 2 times that of BEHB. Again, this agrees with our observation. One may argue that alkyne moieties may form oligomers and polymers when adsorbed on the surface of Ru nanoparticles. However, TG-GC-MS measurements for Ru@EHB, Ru@BEHB, and Ru@DEHB do not show any molecular pieces larger than the ligands, excluding the oligomers and polymers on the Ru nanoparticle surface. In all, the TGA analysis indicates the terminal and internal alkynes might take the binding modes at the metal−ligand interface shown in Scheme 1. The ligand structures on the Ru nanoparticle surface were further examined by ^{1}H NMR measurements in CD_2Cl_2, as shown in Figure S1. One can see that all nanoparticle samples exhibited two main, broad peaks at ca. 0.9 and 1.3 ppm, which are due to the terminal methyl and methylene protons of the respective ligands. More significant broadening can be seen with the peaks for phenyl protons at ca. 7.0 ppm. This is consistent with the binding of the ligands onto the nanoparticle surface via the acetylene moiety, most likely adopting an end-on configuration for Ru@EHB and side-on for Ru@BEHB and Ru@DEHB (Scheme 1). In addition, the fact that only broad NMR features were

Table 1. Summary of TGA and ICP-OES Data of Ru@EHB, Ru@BEHB, and Ru@DEHB Nanoparticles

sample	Ru@EHB	Ru@BHBE	Ru@DEHB
T_g (°C)	271	264	277
Ru weight (%) By TGA	61.1	68.4	82.7
Ru weight (%) by ICP-OES	58.3	65.1	79.3
organic weight (%)	38.9	31.6	17.3
number of ligands	123.6	51.8	21.9
footprint (Å^2)	10.7	27.2	64.4

DOI: 10.1021/acscatal.8b04028
ACS Catal. 2019, 9, 98−104

Table 2. C≡C Vibration in Monomeric Ligands and Ligand-Capped Ru Nanoparticles

sample	EHB	Ru@EHB	BEHB	Ru@BEHB	DEHB	Ru@DEHB
ν (cm^{-1})	2108	**2051**	2141	**1960**	2212	**2046**
		1944			2138	**1950**

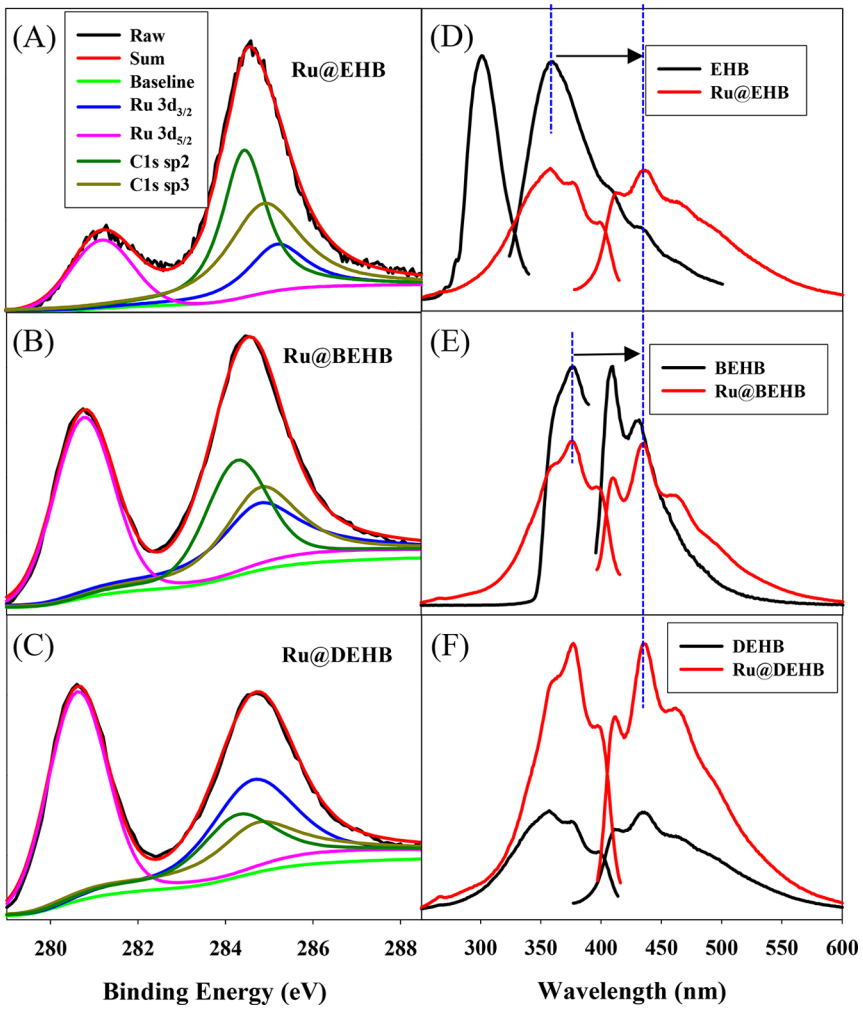

Figure 1. High-resolution XPS spectra of (A) Ru@EHB, (B) Ru@BEHB, and (C) Ru@DEHB nanoparticles. Excitation and emission spectra of (D) EHB and Ru@EHB, (E) BEHB and Ru@BEHB, and (F) DEHB and Ru@DEHB in $CHCl_3$.

observed suggests that the nanoparticles were spectroscopically clean without excess monomeric ligands.[19−21]

The metal−ligand interfacial bonding interactions are further characterized by FTIR spectroscopy and shown in Figure S3. The C≡C bonds for alkyne monomers and related bonds for Ru nanoparticles are listed in Table 2. The absence of ≡C−H stretch at 3299 cm^{-1} for the free ligands of EHB was absent for the Ru@EHB nanoparticles, and the C≡C stretch shifted from 2108 cm^{-1} for EHB ligands to 1944 and 2051 cm^{-1} for Ru@EHB. This has been ascribed to the adsorption of the EHB ligands onto the ruthenium nanoparticle surface in an end-on configuration with a Ru═C═CH- interfacial bonds, as observed previously.[21−24] Similarly, the C≡C vibration red-shifted from 2141 cm^{-1} for free BEHB ligands to 1960 cm^{-1} for Ru@BEHB, and the diacetylene C≡C−C≡C vibrations showed a red-shift from 2215 and 2141 cm^{-1} for the free DEHB ligands[25] to 2046 and 1950 cm^{-1} for Ru@DEHB (Figure S2). This marked discrepancy of wavenumber strongly suggests that the alkyne ligands were indeed chemically bonded onto the Ru surface, and the decreasing bonding order (lower peak wavenumbers) might be attributed to the bonding interactions between the acetylene moieties and the ruthenium metal cores. For the Ru@EHB nanoparticles, this is due to the formation of conjugated metal−ligand interfacial bonds that led to effective intraparticle charge delocalization between the particle-bound acetylene moieties, whereas for the Ru@BEHB and Ru@DEHB nanoparticles, the weakening of the acetylene vibrations can be ascribed to the $\sigma-\pi$ bonds formed by the internal C≡C moiety with the metal nanoparticle surface in a side-on η^2 configuration, as observed previously in surface-enhanced Raman scattering measurements of the terminal alkyne self-assembly on transition-metal surfaces.[24] In such $\delta-\pi$ bonds, the C≡C moiety lies flat onto the metal with the π orbitals directed toward the surface plane such that charge transfer occurs from the Ru d orbital to the C≡C π^* orbital (Scheme 1).

The interfacial bonding interactions of Ru nanoparticles with terminal and internal alkynes were further examined by XPS

DOI: 10.1021/acscatal.8b04028
ACS Catal. 2019, 9, 98−104

Table 3. Excitation and Emission Maxima of Monomeric Ligands and Ligand-Capped Ru Nanoparticles in $CHCl_3$

sample	EHB	Ru@EHB	BEHB	Ru@BEHB	DEHB	Ru@DEHB
λ_{ex} (nm)	302	357	376	375	377	377
λ_{em} (nm)	358	436	409	435	432	437
$\Delta\lambda$ (nm)		**78**		**26**		**5**

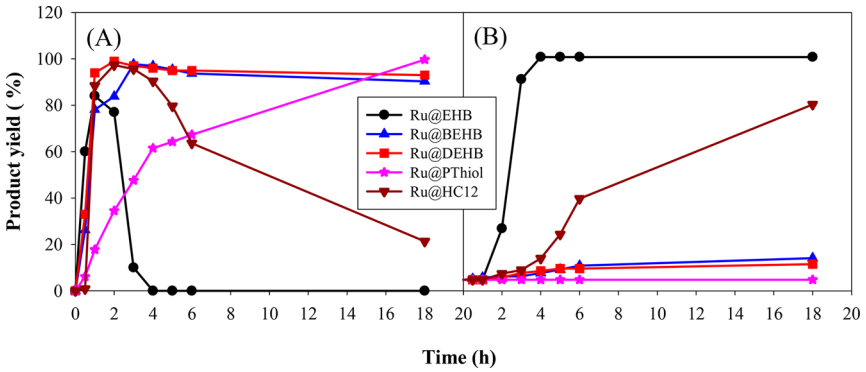

Figure 2. Evolution of hydrogenation of styrene products, (A) ethylbenzene and (B) ethylcyclohexane, catalyzed by Ru@EHB (black ●), Ru@BEHB (blue ▲), Ru@DEHB (red ■), Ru@PThiol (pink ◆), and Ru@HC12 (magenta ▼).

measurements. Figure 1A–C show the high-resolution XPS spectra of the C 1s and Ru 3d electrons of Ru@EHB, Ru@BEHB, and Ru@DEHB nanoparticles, respectively. Deconvolution yields a pair of peaks at 284.9 and 284.4 eV, which are due to sp^3 and sp^2 C 1s electrons, respectively,[26] and the binding energies of Ru $3d_{5/2}$ for Ru@EHB, Ru@BEHB, and Ru@DEHB nanoparticles was observed at 281.0, 280.75, and 280.6 eV, respectively, showing a positive shift of 0.80 eV, 0.55, and 0.4 eV, respectively, as compared with that of metallic ruthenium (280.2 eV).[27,28] Such high binding energy of Ru 3d5/2 for Ru@EHB nanoparticles might be due to the nanosized Ru cores and strong electron-withdrawing groups of phenyl ring through Ru═C═CH bonds, as demonstrated in earlier studies.[15,29,30]

The discrepancy of the interfacial bonding between terminal and internal alkynes onto Ru metal nanoparticles was found to lead to a marked difference of the nanoparticle photoluminescence properties. Figure 1D–F displays the excitation and emission spectra of Ru@EHB, Ru@BEHB, and Ru@DEHB nanoparticles, along with those of the respective ligands. The wavelengths of the excitation and emission maxima derived from these spectra are listed in Table 3. It can be seen that free EHB monomers exhibited an excitation maximum (λ_{ex}) at 302 nm and a corresponding emission maximum (λ_{em}) at 358 nm, whereas for Ru@EHB they red-shifted markedly to 357 and 436 nm, respectively, close to those of the DEHB (377 and 432 nm), consistent with the formation of Ru═C═CH− conjugated bonds that led to intraparticle charge delocalization between the particle-bound acetylene moieties and hence analogous behaviors to the dimeric counterparts, as observed previously.[7,31] By sharp contrast, the λ_{ex} and λ_{em} for Ru@DEHB are almost identical to those of DEHB, suggesting that side-on interactions of the DEHB ligands to the nanoparticle surface did not lead to an appreciable change of the ligand electronic energy. For Ru@BEHB, whereas the λ_{ex} was almost unchanged as compared to that of BEHB, the λ_{em} showed a moderate red-shift of ca. 26 nm, suggesting that the Ru-BEHB interfacial bonding interactions were in the intermediate between those of Ru-EHB and Ru-DEHB.

Previously, Philippot et al. studied styrene hydrogenation catalyzed by PVP-capped ruthenium (Ru@PVP) nanoparticles and found that the molecule adsorbed onto the Ru@PVP surface through the vinyl groups rather than the phenyl end[32] and hydrogenation of the phenyl rings requires π coordination of the phenyl groups.[33,34] When the Ru nanoparticle surface was coordinated with CO groups in a bridging mode (CO bridging sites), hydrogenation of the phenyl ring was substantially impeded, while the activity toward hydrogenation of the vinyl group was slowed down slightly, as compared with that of CO-free Ru nanoparticles. When completely saturated with CO, Ru@PVP nanoparticles displayed no activity toward either vinyl or phenyl group.[35,36] The authors further concluded that the CO-bridging sites are responsible for the hydrogenation of phenyl groups.[32]

As shown in Figure 2 and Table S2, ruthenium nanoparticles capped with terminal and internal alkynes showed markedly different behaviors to each other. In contrast to the sequential hydrogenation of the vinyl and phenyl groups of styrene by Ru@EHB nanoparticles, Ru@DEHB and Ru@BEHB are active only toward hydrogenation of the vinyl group, while almost inert to the hydrogenation of the phenyl group. Such discrepancy of the catalytic selectivity between ruthenium nanoparticles capped with internal alkynes (i.e., Ru@BEHB and Ru@DEHB) and those functionalized with terminal alkynes (i.e., Ru@EHB) can be explained with this scenario. The C≡C moieties in BEHB and DEHB ligands take the bridging sites on Ru nanoparticles surface through η^2 σ–π bonds of C≡C and behave analogously to the CO on the bridging sites, thus preventing the hydrogenation of phenyl group. By contrast, EHB tautomerized to vinylidene moieties and preferred to take the hollow site on Ru nanoparticle surface in the end-on mode. In addition, the π–π staking among the phenyl groups of EBH ligands led to the formation of EHB molecular bundles and makes the styrene more accessible to the Ru sites.[37,38]

Consistent results were obtained in DFT calculations where we examined the adsorption of terminal and internal alkynes on Ru metal surface, as shown in Supporting Information (Figure S6–10). Figure S6 shows the transition states,

DOI: 10.1021/acscatal.8b04028
ACS Catal. 2019, 9, 98–104

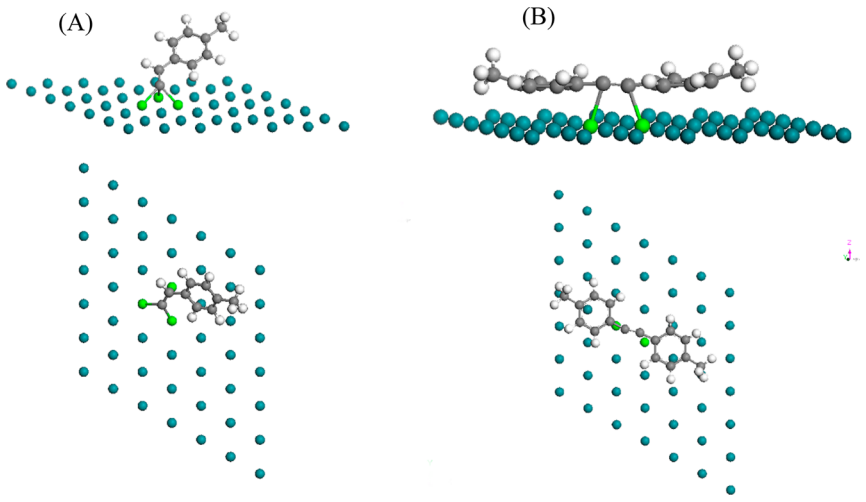

Figure 3. Adsorption configurations of terminal alkyne 4-ethynyltoluene (A) and internal alkyne 1,2-di-*p*-tolylethyne (B) on Ru (0001). The Ru atoms bonding with carbon atoms are highlighted with green color. The adsorption energy in (A) is −4.07 eV and that in (B) is −4.40 eV. The adsorption energy is defined as E_{ads}= E(mol/sur) − E(sur) − E(mol), where $E_{(mol/sur)}$ is the energy of the system of the adsorbate taking the optimized configuration on Ru metal surface. $E_{(mol)}$ is the energy of the free molecule of the adsorbate. $E_{(sur)}$ is the energy of the metal surface without any adsorbate.

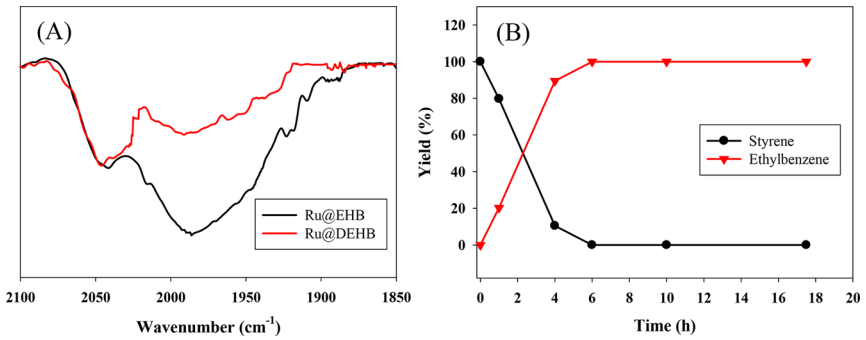

Figure 4. (A) In situ FTIR spectra of Ru@EHB and Ru@DEHB nanoparticles poisoned for 4 h in 1 atm CO atmosphere; (B) Evolution of hydrogenation products of styrene by Ru@EHB poisoned with CO.

molecular configurations, and the energy barriers for the transformation of adsorbed 1-propyne on Ru(0001) to the vinylidene (**#1** to **#9**). Although the energy of (**#3**) is slightly lower than **#9** and one can argue that **#9** is more preferred than vinylidene (**#9**), it is possible that when many terminal alkyne molecules adsorbed on Ru metal surfaces, H from any other molecules could be present at the Hc site for CH3CC* and form #7, rendering the tautomerization of terminal alkyne to vinylidene exothermic and spontaneous.

Most importantly, the DFT calculation (Figure 3) indicates that internal alkyne moieties adsorb on the Ru surface via the bridging site and thus block the active site for the hydrogenation of phenyl group. Instead, terminal alkyne moieties adsorb on Ru surface in side-on mode, further tautomerize to vinylidene and take the hollow site in end-on mode, thus leaving the bridging site available for the hydrogenation of phenyl group. Thus, the DFT calculation results agree well with our anticipation and support the catalytic performance of Ru@EHB, Ru@BEHB, and Ru@DEHB nanoparticles.

Figure 4A shows the in situ FTIR spectra of Ru@EHB and Ru@DEHB nanoparticles poisoned in 1 MPa CO atmosphere for 4 h. It can be observed that the ratio of the intensity of CO-bridging (1980 cm^{-1}) to CO-top (2050 cm^{-1})[39] for Ru@EHB is much higher than that of Ru@DEHB, suggesting that Ru@EHB nanoparticles contained more CO-bridging sites than that the CO-top sites and thus show high selectivity toward styrene hydrogenation. In Figure 4B and Figure S11, catalysis test shows that the CO poisoned Ru@EHB nanoparticles lost the ability of producing cyclohexane, and the reaction rate of producing ethylbenzene by Ru@EHB and Ru@DEHB were much slower. To prevent the possible aggregation of Ru nanoparticles during catalysis reaction and further on the selectivity of hydrogenation of styrene by Ru@EHB and Ru@DEHB nanoparticles, we further did the TEM for Ru@DEHB after catalysis and also repeated the catalysis reaction for both Ru@EHB and Ru@DEHB. The size of Ru@DEHB after catalysis is 1.8 ± 0.2 nm (Figure S4-D), which is consistent with that of the as-prepared Ru@DEHB (1.7 ± 0.3). As shown in Figure S12, the selectivity of hydrogenation by Ru@EHB and Ru@DEHB in the second run is quite similar to that in the first, thus excluding the possibility of the aggregation of Ru nanoparticles on the selectivity of hydrogenation of styrene.

In addition, as EHB moieties adsorbed on Ru@EHB nanoparticles in the end-on mode and molecular bundles, more space was available for the accessibility of styrene and hydrogenation. By contrast, BEHB and DEHB take the side-on mode on both Ru@BEHB and Ru@DEHB nanoparticles surfaces. Whereas an increasing fraction of Ru nanoparticles surface is not directly bonded with ligands, the accessibility of

DOI: 10.1021/acscatal.8b04028
ACS Catal. 2019, 9, 98−104

styrene to these unbonded Ru surfaces could was impeded by the hexylbenzene fragments of the capping ligands that adopted the side-on mode (Scheme 1), thus preventing the hydrogenation of styrene.

Ru@HC12, sharing the same Ru═CH═C interfacial bonds but different molecular structure of capping ligands with Ru@EHB, are still highly active to both vinyl and phenyl hydrogenation and behave similarly to that of Ru@EHB. However, the reaction dynamics of hydrogenation of phenyl groups for Ru@HC12 is largely slowed as compared to that of Ru@EHB, which might be caused by the steric effect of the long alkyl chain, preventing the effective access of the phenyl ring of styrene to and formation of π coordination with the Ru metal surface. For Ru@PThiol nanoparticles, although PThiol ligands took the upright position on Ru nanoparticles surface, Ru nanoparticles behaved much like that of partially CO-poisoned ruthenium nanoparticles, with much slowed hydrogenation of vinyl and completely suppressed activity toward hydrogenation of phenyl group.[35,36] This might suggest that the inactivity of ruthenium nanoparticles capped with moieties of internal alkynes are mainly caused by the occupation of the bridging sites of ruthenium nanoparticles surfaces by C≡C triple bonds of internal alkynes.

CONCLUSION

In summary, ruthenium nanoparticles capped with terminal and internal alkyne ligands were prepared and the Ru-acetylene interfacial bonding interactions were examined by TGA, ^{1}H NMR, FTIR, XPS, photoluminescence measurements, and DFT calculation. The results suggest that internal alkyne adopted an η^2 side-on configuration, forming $\delta-\pi$ covalent bonds on Ru nanoparticle surface. Such interfacial bonds were somewhat weaker than that with terminal alkynes, where Ru═C═CH− interfacial bonds were formed and extensive charge delocalization occurred among the particle-bound acetylene moieties. Interestingly, the Ru nanoparticles capped with terminal alkynes exhibited apparent catalytic activity toward hydrogenation of both the vinly and phenyl groups of styrene, while Ru nanoparticle capped with internal alkynes exhibited activity toward the vinyl group only. This discrepancy of catalytic behavior caused by the capping alkynes was accounted for by the combined FTIR and catalysis tests of CO-poisoned Ru nanoparticles, which suggests that the bridging sites might be responsible for the hydrogenation of phenyl group by Ru nanoparticles capped with terminal alkynes.

ASSOCIATED CONTENT

Supporting Information

The Supporting Information is available free of charge on the ACS Publications website at DOI: 10.1021/acscatal.8b04028.

Detailed description of synthesis of BEHB and DEHB monomers, Ru nanoparticles; ^{1}H, ^{13}C NMR, and FTIR spectra of the EHB, BEHB and DEHB monomers; ^{1}H NMR, FTIR spectra, TGA, TEM images of Ru nanoparticles capped with EHB, BEHB, DEHB; and DFT calculation for the transition state of tautomerization of terminal alkyne to vinylidene and the adsorption mode of terminal and internal alkyne on the Ru (0001) surface (PDF)

AUTHOR INFORMATION

Corresponding Authors

*E-mail: esxkang@scut.edu.cn.
*E-mail: shaowei@ucsc.edu.

ORCID

Zhang Lin: 0000-0002-6600-2055
Zhenqing Shi: 0000-0003-1721-5369
Xiongwu Kang: 0000-0003-2587-4962
Shaowei Chen: 0000-0002-3668-8551

Author Contributions

¶(F.Z., J.F., L.H.) These authors contributed equally.

Notes

The authors declare no competing financial interest.

ACKNOWLEDGMENTS

This work was supported by the National Natural Science Foundation of China (No. 51602106), the Fundamental Research Funds for Central Universities (SCUT Grant No. 2017MS066 and 2017MS006). Z.L. would like to thank the Guangdong Innovative and Entrepreneurial Research Team Program (No. 2016ZT06N569).

REFERENCES

(1) Grunes, J.; Zhu, A.; Somorjai, G. A. Catalysis and Nanoscience. *Chem. Commun.* **2003**, 2257−2260.
(2) Xiong, Y. J.; Wiley, B.; Xia, Y. N. Nanocrystals with Unconventional Shapes - A Class of Promising Catalysts. *Angew. Chem., Int. Ed.* **2007**, *46*, 7157−7159.
(3) Astruc, D.; Lu, F.; Aranzaes, J. R. Nanoparticles as Recyclable Catalysts: The Frontier between Homogeneous and Heterogeneous Catalysis. *Angew. Chem., Int. Ed.* **2005**, *44*, 7852−7872.
(4) Somorjai, G. A.; Li, Y. M. Selective Nanocatalysis of Organic Transformation by Metals: Concepts, Model Systems, and Instruments. *Top. Catal.* **2010**, *53*, 832−847.
(5) Zaera, F. Nanostructured Materials for Applications in Heterogeneous Catalysis. *Chem. Soc. Rev.* **2013**, *42*, 2746−2762.
(6) Martinez-Prieto, L. M.; Chaudret, B. Organometallic Ruthenium Nanoparticles: Synthesis, Surface Chemistry, and Insights into Ligand Coordination. *Acc. Chem. Res.* **2018**, *51*, 376−384.
(7) Hu, P. G.; Chen, L. M.; Kang, X. W.; Chen, S. W. Surface Functionalization of Metal Nanoparticles by Conjugated Metal-Ligand Interfacial Bonds: Impacts on Intraparticle Charge Transfer. *Acc. Chem. Res.* **2016**, *49*, 2251−2260.
(8) Tschan, M. J. L.; Diebolt, O.; van Leeuwen, P. W. N. M. Ruthenium Metal Nanoparticles in Hydrogenation: Influence of Phosphorus-Ligands. *Top. Catal.* **2014**, *57*, 1054−1065.
(9) Lara, P.; Philippot, K.; Chaudret, B. Organometallic Ruthenium Nanoparticles: A Comparative Study of the Influence of the Stabilizer on their Characteristics and Reactivity. *ChemCatChem* **2013**, *5* (1), 28−45.
(10) Schoenbaum, C. A.; Schwartz, D. K.; Medlin, J. W. Controlling the Surface Environment of Heterogeneous Catalysts Using Self-Assembled Monolayers. *Acc. Chem. Res.* **2014**, *47*, 1438−1445.
(11) Niu, Z. Q.; Li, Y. D. Removal and Utilization of Capping Agents in Nanocatalysis. *Chem. Mater.* **2014**, *26*, 72−83.
(12) Li, G.; Jin, R. C. Gold Nanocluster-Catalyzed Semihydrogenation: A Unique Activation Pathway for Terminal Alkynes. *J. Am. Chem. Soc.* **2014**, *136*, 11347−11354.
(13) Wang, Y.; Wan, X. K.; Ren, L. T.; Su, H. F.; Li, G.; Malola, S.; Lin, S. C.; Tang, Z. C.; Hakkinen, H.; Teo, B. K.; Wang, Q. M.; Zheng, N. F. Atomically Precise Alkynyl-Protected Metal Nanoclusters as a Model Catalyst: Observation of Promoting Effect of Surface Ligands on Catalysis by Metal Nanoparticles. *J. Am. Chem. Soc.* **2016**, *138*, 3278−3281.

DOI: 10.1021/acscatal.8b04028
ACS Catal. 2019, 9, 98−104

(14) Wan, X. K.; Wang, J. Q.; Nan, Z. A.; Wang, Q. M. Ligand Effects in Catalysis by Atomically Precise Gold Nanoclusters. *Sci. Adv.* **2017**, *3*, e1701823.
(15) Chen, W.; Lin, T. J.; Dai, Y. Y.; An, Y. L.; Yu, F.; Zhong, L. S.; Li, S. G.; Sun, Y. H. *Recent Advances in the* Investigation of Nanoeffects of Fischer−Tropsch Catalysts. *Catal. Today* **2018**, *311*, 8−22.
(16) Astruc, D. *Nanoparticles and Catalysis*; Wiley-VCH: Weinheim, 2008; pp xxiii, 640.
(17) Tulevski, G. S.; Myers, M. B.; Hybertsen, M. S.; Steigerwald, M. L.; Nuckolls, C. Formation of Catalytic Metal-Molecule Contacts. *Science* **2005**, *309*, 591−594.
(18) Bruneau, C.; Dixneuf, P. H. Metal Vinylidenes in Catalysis. *Acc. Chem. Res.* **1999**, *32*, 311−323.
(19) Chen, W.; Davies, J. R.; Ghosh, D.; Tong, M. C.; Konopelski, J. P.; Chen, S. W. Carbene-Functionalized Ruthenium Nanoparticles. *Chem. Mater.* **2006**, *18*, 5253−5259.
(20) Hostetler, M. J.; Wingate, J. E.; Zhong, C. J.; Harris, J. E.; Vachet, R. W.; Clark, M. R.; Londono, J. D.; Green, S. J.; Stokes, J. J.; Wignall, G. D.; Glish, G. L.; Porter, M. D.; Evans, N. D.; Murray, R. W. Alkanethiolate Gold Cluster Molecules with Core Diameters from 1.5 to 5.2 nm: Core and Monolayer Properties as a Function of Core Size. *Langmuir* **1998**, *14*, 17−30.
(21) Kang, X. W.; Zuckerman, N. B.; Konopelski, J. P.; Chen, S. W. Alkyne-Functionalized Ruthenium Nanoparticles: Ruthenium-Vinylidene Bonds at the Metal-Ligand Interface. *J. Am. Chem. Soc.* **2012**, *134*, 1412−1415.
(22) Hu, P. G.; Chen, L. M.; Deming, C. P.; Bonny, L. W.; Lee, H. W.; Chen, S. W. Identification of the Formation of Metal-Vinylidene Interfacial Bonds of Alkyne-Capped Platinum Nanoparticles by Isotopic Labeling. *Chem. Commun.* **2016**, *52*, 11631−11633.
(23) Patterson, M. L.; Weaver, M. J. Surface-Enhanced Raman Spectroscopy as a Probe of Adsorbate-Surface Bonding: Simple Alkenes and Alkynes Adsorbed at Gold Electrodes. *J. Phys. Chem.* **1985**, *89*, 5046−5051.
(24) Feilchenfeld, H.; Weaver, M. J. Binding of Alkynes to Silver, Gold, and Underpotential Deposited Silver Electrodes as Deduced by Surface-Enhanced Raman Spectroscopy. *J. Phys. Chem.* **1989**, *93*, 4276−4282.
(25) Tammer, M.; Sokrates, G. Infrared and Raman Characteristic Group Frequencies: Tables and Charts. *Colloid Polym. Sci.* **2004**, *283* (2), 235.
(26) Kang, X. W.; Chen, S. W. Electronic Conductivity of Alkyne-Capped Ruthenium Nanoparticles. *Nanoscale* **2012**, *4*, 4183−4189.
(27) Chakroune, N.; Viau, G.; Ammar, S.; Poul, L.; Veautier, D.; Chehimi, M. M.; Mangeney, C.; Villain, F.; Fievet, F. Acetate- and Thiol-Capped Monodisperse Ruthenium Nanoparticles: XPS, XAS, and HRTEM Studies. *Langmuir* **2005**, *21*, 6788−6796.
(28) Luque, R.; Clark, J. H.; Yoshida, K.; Gai, P. L. Efficient Aqueous Hydrogenation of Biomass Platform Molecules Using Supported Metal Nanoparticles on Starbons (R). *Chem. Commun.* **2009**, *35*, 5305−5307.
(29) Zhou, Z. Y.; Kang, X. W.; Song, Y.; Chen, S. W. Ligand-Mediated Electrocatalytic Activity of Pt Nanoparticles for Oxygen Reduction Reactions. *J. Phys. Chem. C* **2012**, *116*, 10592−10598.
(30) Mercurio, G.; McNellis, E. R.; Martin, I.; Hagen, S.; Leyssner, F.; Soubatch, S.; Meyer, J.; Wolf, M.; Tegeder, P.; Tautz, F. S.; Reuter, K. Structure and Energetics of Azobenzene on Ag(111): Benchmarking Semiempirical Dispersion Correction Approaches. *Phys. Rev. Lett.* **2010**, *104*, 036102.
(31) Chen, W.; Zuckerman, N. B.; Lewis, J. W.; Konopelski, J. P.; Chen, S. W. Pyrene-Functionalized Ruthenium Nanoparticles: Novel Fluorescence Characteristics from Intraparticle Extended Conjugation. *J. Phys. Chem. C* **2009**, *113*, 16988−16995.
(32) Novio, F.; Monahan, D.; Coppel, Y.; Antorrena, G.; Lecante, P.; Philippot, K.; Chaudret, B. Surface Chemistry on Small Ruthenium Nanoparticles: Evidence for Site Selective Reactions and Influence of Ligands. *Chem. - Eur. J.* **2014**, *20*, 1287−1297.
(33) Lara, P.; Rivada-Wheelaghan, O.; Conejero, S.; Poteau, R.; Philippot, K.; Chaudret, B. Ruthenium Nanoparticles Stabilized by N-Heterocyclic Carbenes: Ligand Location and Influence on Reactivity. *Angew. Chem., Int. Ed.* **2011**, *50*, 12080−12084.
(34) Gonzalez-Galvez, D.; Lara, P.; Rivada-Wheelaghan, O.; Conejero, S.; Chaudret, B.; Philippot, K.; van Leeuwen, P. W. N. M. NHC-stabilized Ruthenium Nanoparticles as New Catalysts for the Hydrogenation of Aromatics. *Catal. Sci. Technol.* **2013**, *3*, 99−105.
(35) Chen, C. S.; Lin, J. H.; Chen, H. W.; Wang, C. Y. Infrared Study of Benzene Hydrogenation on Pt/SiO2 Catalyst by Co-adsorption of CO and Benzene. *Catal. Lett.* **2005**, *105*, 149−155.
(36) Hammer, B.; Nielsen, O. H.; Norskov, J. K. Structure Sensitivity in Adsorption: CO Interaction with Stepped and Reconstructed Pt Surfaces. *Catal. Lett.* **1997**, *46*, 31−35.
(37) Wu, S. M.; Gonzalez, M. T.; Huber, R.; Grunder, S.; Mayor, M.; Schonenberger, C.; Calame, M. Molecular Junctions Based on Aromatic Coupling. *Nat. Nanotechnol.* **2008**, *3*, 569−574.
(38) Favier, I.; Massou, S.; Teuma, E.; Philippot, K.; Chaudret, B.; Gomez, M. A New and Specific Mode of Stabilization of Metallic Nanoparticles. *Chem. Commun.* **2008**, 3296−3298.
(39) Novio, F.; Philippot, K.; Chaudret, B. Location and Dynamics of CO Co-ordination on Ru Nanoparticles: A Solid State NMR Study. *Catal. Lett.* **2010**, *140*, 1−7.

DOI: 10.1021/acscatal.8b04028
ACS Catal. 2019, 9, 98−104